Journal Pre-proofs

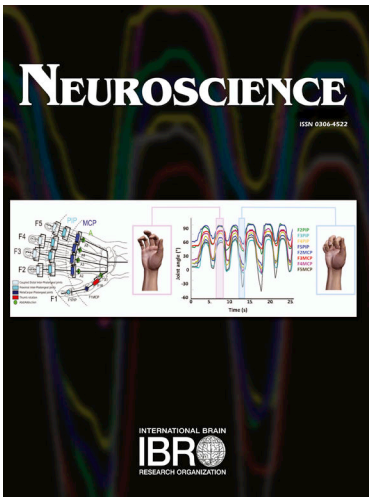

Research Article

Biomarkers derived from alterations in overlapping community structure of resting-state brain functional networks for detecting Alzheimer's disease

Hongfang Han, Xuan Li, John Q. Gan, Hua Yu, Haixian Wang, and for the Alzheimer's Disease Neuroimaging Initiative,

PII: S0306-4522(21)00662-X
DOI: https://doi.org/10.1016/j.neuroscience.2021.12.031
Reference: NSC 20470

To appear in: *Neuroscience*

Received Date: 25 June 2021
Revised Date: 17 December 2021
Accepted Date: 23 December 2021

Please cite this article as: H. Han, X. Li, J.Q. Gan, H. Yu, H. Wang, and for the Alzheimer's Disease Neuroimaging Initiative, Biomarkers derived from alterations in overlapping community structure of resting-state brain functional networks for detecting Alzheimer's disease, *Neuroscience* (2021), doi: https://doi.org/10.1016/j.neuroscience.2021.12.031

Biomarkers derived from alterations in overlapping community structure of resting-state brain functional networks for detecting Alzheimer's disease

Hongfang Han[a,b,1], Xuan Li[a,c,d,1], John Q. Gan[c], Hua Yu[e], Haixian Wang[a,b,*], and for the Alzheimer's Disease Neuroimaging Initiative[2]

[a]*Key Laboratory of Child Development and Learning Science of Ministry of Education, School of Biological Science & Medical Engineering, Southeast University, Nanjing 210096, Jiangsu, PR China*
[b]*Institute of Artificial Intelligence of Hefei Comprehensive National Science Center, Hefei 230094, Anhui, PR China*
[c]*School of Computer Science and Electronic Engineering, University of Essex, Colchester CO4 3SQ, UK*
[d]*Institute of Neuroscience and Medicine (INM-7: Brain and Behaviour), Research Centre Jülich, 52425 Jülich, Germany*
[e]*Department of Cardiology, The First Affiliated Hospital of USTC, Division of Life Sciences and Medicine, University of Science and Technology of China, Hefei 230001, Anhui, PR China*

Abstract

Recent studies show that overlapping community structure is an important feature of the brain functional network. However, alterations in such overlapping community structure in Alzheimer's disease (AD) patients have not been examined yet. In this study, we investigate the overlapping community structure in AD by using resting-state functional magnetic resonance imaging (rs-fMRI) data. The collective sparse symmetric non-negative matrix factorization (cssNMF) is adopted to detect the overlapping community structure. Experimental results on 28 AD patients and 32 normal controls (NCs) from the ADNI2 dataset show that the two groups have remarkable differences in terms of the optimal number of communities, the hierarchy of communities detected at different scales, network functional segregation, and nodal functional diversity. In particular, the frontal-parietal and basal ganglia networks exhibit significant differences between the two groups. A machine learning framework proposed in this paper for AD detection achieved an accuracy of 76.7% when using the detected community strengths of the frontal-parietal and basal ganglia networks only as input features. These findings provide novel insights into the understanding of pathological changes in the brain functional network organization of AD and show the potential of the community structure-related features for AD detection.

Keywords: Alzheimer's disease, overlapping community structure, brain functional network, resting-state fMRI, machine learing, agglomerative hierarchical clustering

Introduction

Alzheimer's disease (AD) is a common prevalent neurodegenerative disorder, characterized by memory and cognitive function impairment. Resting state functional magnetic resonance imaging (rs-fMRI) provides

*Corresponding author.
Email address: hxwang@seu.edu.cn (Haixian Wang)
[1]Co-first authors. Hongfang Han and Xuan Li are the co-first authors of the article.
[2]Data used in preparation of this article were obtained from the Alzheimer's Disease Neuroimaging Initiative (ADNI) database (adni.loni.usc.edu). As such, the investigators within the ADNI contributed to the design and implementation of ADNI and/or provided data but did not participate in analysis or writing of this report. A complete listing of ADNI investigators can be found at: http://adni.loni.usc.edu/wp-content/uploads/how_to_apply/ADNI_Acknowledgement_List.pdf

a useful way to study the subtle brain abnormalities in AD (Dennis and Thompson, 2014; de Vos et al., 2018). Some studies based on rs-fMRI indicate that the changes in brain function may occur before obvious clinical symptoms or structural damage (Pievani et al., 2011; Teipel et al., 2015). In studies of the brain function, graph theory analysis provides a promising theoretical tool for understanding the brain network organization. Typically, the brain functional network comprises nodes and edges, which are defined as brain regions and their interactions, respectively. Such interactions (i.e., associations among the brain regions) reflect the temporal dependency of the time series of different brain regions, termed as functional connectivity (Biswal et al., 1995). Various studies suggest that the framework of the brain functional network and graph theory analysis has great potentials in diagnosing neurological diseases (Fornito et al., 2015; de Vos et al., 2018). For AD, abnormal connectivity patterns have been observed based on network association matrices constructed by different methods (Noroozi and Rezghi, 2020; Sun et al., 2021). Besides, graph measures, such as the rich-club and clustering coefficient, have been adopted to reveal the pathology of AD (Li et al., 2019; Xue et al., 2020).

In particular, community structure of the brain functional network offers a valuable tunnel to study the function of both normal and abnormal brains. Community structure is one of the most essential topological features of the brain functional network. A community (or module) of the brain functional network is a cluster of highly connected nodes with only weak connections among the different clusters. Such community structure plays an important role in maintaining the efficiency of information communication, by balancing the functional segregation and information integration via hubs, where functional segregation refers to the efficiency of information exchange among functionally related regions within the modules and functional integration measures the efficiency of global communication (Sporns, 2013). The community structure has been found to change with age and cognitive ability (Crossley et al., 2013; Wen et al., 2018).In addition, community structure-related features of brain structural networks in AD patients have been investigated and used for AD classification (Prasad et al., 2015; John et al., 2017; Hojjati et al., 2019). A decreased number of larger communities in the AD patients compared to the healthy group has been found in (Contreras et al., 2019). Furthermore, disrupted modular organization and information communication in AD have been consistently discovered by various studies using different modalities and computational methods (Dai and He, 2014). These studies suggest that community structure-related features might be potentially useful for AD detection. However, most AD studies focus on non-overlapping community structures. In fact, many studies suggest that the brain functional network, like many other real-world complex networks, have an overlapping community structure (Palla et al., 2005; O'Reilly et al., 2010; Cole et al., 2013).

In an overlapping community structure, one brain region could participate in more than one communities. Several recent algorithms for overlapping community structure detection have been applied to rs-fMRI data (Wu et al., 2011; Najafi et al., 2016; Lin et al., 2018). In this work, we deploy the collective sparse symmetric non-negative matrix factorization (cssNMF) method to detect the overlapping community structure, which has been proposed in our previous work (Li et al., 2018). The cssNMF method operates on a weighted brain functional network. The advantage of this method is that it not only identifies the group-level overlapping community structure across multiple participants, but also preserves the individual differences in terms of community strengths. Such inter-participant variation in the communities can be further used as classification features for AD detection.

This study aims to investigate the changes in the overlapping community structure of AD patients.

Specifically, the overlapping community structure is detected by using cssNMF with non-negative adaptive sparse representation (NASR), which has been proposed in our previous work (Li and Wang, 2015; Li et al., 2018). The community structure is studied in different aspects, including the optimal number of communities, reproducibility, network functional segregation, and nodal functional diversity. In particular, we studied the hierarchy of communities detected at different scales, by using the agglomerative hierarchical clustering (Hastie et al., 2009). Furthermore, we proposed a machine learning framework to deploy the community-structure-based features for AD detection. We expect this study to provide novel insights into the community structure of the brain functional network in AD, and explore potential biomarkers for AD detection.

Methods and Materials

Participants and data acquisition

All participants aged from 60 to 90 years old in the Alzheimer's Disease Neuroimaging Initiative (ADNI-2) during the screening visit (`http://adni.loni.usc.edu`) were analyzed in this study. All participants were divided into a patient group and a normal control (NC) group. Participants with a mild to moderate level of AD measured by the mini-mental state examination (MMSE) score ranging from 14 to 26 and the clinical dementia rating (CDR) score of 0.5 or 1 were selected into the AD group. Healthy participants in the NC group had an MMSE score ranging from 27 to 30 with CDR=0. All the participants were exclusive of Parkinson's disease and depression, and all the AD participants were diagnosed as probable AD. It resulted in a dataset of 69 participants (31 AD patients and 38 healthy participants).

All rs-fMRI and structural magnetic resonance imaging (sMRI) images used in this work were acquired by Philips scanners following the ADNI acquisition protocol (Jack et al., 2008), with a repetition time (TR) of 3 s and a field strength of 3.0 T. Details of the scanning parameters are available from `http://adni.loni.usc.edu`. Informed consent was obtained from all the individual participants included in the study.

Data preprocessing

The rs-fMRI and sMRI images were preprocessed by using the Data Processing Assistant for Resting-State fMRI (DPARSF) toolbox (Yan and Zang, 2010) in MATLAB 2020b, following the widely-accepted pipelines. Specifically, for each participant, the first 7 of all the 140 echoplanar imaging (EPI) volumes were discarded for signal equilibrium. Slice timing correction and realignment for head motion correction were performed on the remaining volumes. For each voxel, the time series were detrended with the Friston-24 head motion parameters, cerebrospinal fluid (CSF) and white matter (WM) signals were regressed out. Afterwards, the T1-weighted image was coregistered to the mean functional image. Normalization to the Montreal Neurological Institute (MNI) space was performed by using the DARTEL procedure. The signals were then spatially smoothed with a 6 mm full width half maximum (FWHM) Gaussian kernel and bandpass filtered (0.01-0.08Hz). In terms of head motion, 9 participants were excluded under the inclusion criteria because the number of frames (with framewise displacement (FD) > 0.5 (Power et al., 2011)) was more than 50, and the overall head motion was more than 2 mm or 2 degree. The t-test was performed on the FD parameters of the AD and NC groups. The result ($p > 0.05$) reveals no significant difference in head movement between the two groups. This resulted in a dataset of 60 participants in total (28 AD patients and 32 NCs). Finally, the

whole-brain was partitioned into 90 regions of interest (ROIs) according to the automated anatomical labeling (AAL) template (Tzourio-Mazoyer et al., 2002), and the mean time series over all voxels were extracted for each ROI. Besides, the AD patients (13 female, mean age: 73.8 ± 6.1 yrs, education level: 16.1 ± 2.9 yrs) and the NCs (19 female, mean age: 74.4 ± 5.7 yrs, education level: 16.3 ± 2.0 yrs) were matched in age, sex and education level.

Functional connectivity

For the computation of functional connectivity, we adopted the NASR method, instead of using the Pearson correlation method. In our previous work, we have shown that the detected communities benefit from the NASR-based connectomes compared to the Pearson correlation-based connectome, by achieving better reproducibility and interpretability (Li and Wang, 2015). The main difference between these two methods is that NASR takes into account the influence from the other nodes when computing functional connectivity. In other words, it computes the associations between one node with all the other nodes simultaneously, rather than calculates the pairwise associations. Besides, NASR produces non-negative and sparse functional connectivity, as it automatically preserves only the most important connections, with the advantage of improving the interpretability and reducing the data complexity. Therefore, we applied the NASR method to compute functional connectivity in this work. The code for implementing the NASR algorithm is available in `https://github.com/xuanli-ac/NASR`. As a result, we derived a symmetric 90×90 association matrix for each participant, representing the functional connectome.

Overlapping community structure detection

We applied the cssNMF method (Li et al., 2018) for the community detection, as it identifies the group-level overlapping community structure across multiple participants while maintaining individual differences in community strength. Briefly, given the non-negative association matrices of a set of participants, i.e., $\mathrm{G}^i \in \mathbb{R}^{n \times n}$ $(i = 1, \ldots, m)$ where n and m denote the number of nodes and the number of participants respectively, cssNMF detects the community structure by optimizing the following objective function:

$$\begin{aligned} &\min_{\mathrm{H,S} \geq 0} \frac{1}{2} \sum_{i=1}^{m} \|\mathrm{G}^i - \mathrm{H}\mathrm{S}^i\mathrm{H}^{\mathrm{T}}\|_{\mathrm{F}}^2 + \beta \|\mathrm{H}\|_1 \\ &s.t.\ \forall p : \max(h_p) = 1, p = 1, \ldots, k. \end{aligned} \tag{1}$$

The detected group-level communities are represented in $\mathrm{H} = (h_1, \ldots, h_k) \in \mathbb{R}^{n \times k}$, where each element H_{ij} reflects the weight of node i in community j and k is the number of detected communities. The individual differences are preserved in the diagonal matrix $\mathrm{S}^i = \mathrm{diag}(s^i) \in \mathbb{R}^{k \times k}$ with $s^i \in \mathbb{R}^k$, where s_p^i is the average connection strength of the nodes of community p in the network of participant i and indicates the expression level of community p in participant i. The regularization parameter $\beta > 0$ controls the sparsity of the H, i.e., the number of nodes participating in a community. The code for implementing the cssNMF algorithm is available in `https://github.com/xuanli-ac/cssNMF`.

Grid searches with 2-fold cross-validation were adopted to determine the parameters k and β for community detection as done by (Li et al., 2018), where k ranges from 2 to 16 and β ranges from 0 to 1 with a step size of 0.1. Among them, the range for value k was selected according to previous studies (Van den Heuvel and Pol, 2010; Yeo et al., 2011; Wu et al., 2011; Yeo et al., 2014; Najafi et al., 2016; Mirzaei and Soltanian-Zadeh,

2019). Besides, for each computation, 20 runs with random initializations were performed to select the best result with the minimum value of the objective function.

Analysis of group-level differences in community structure

Number of detected communities

Firstly, we investigated whether the optimal number of communities differs between the AD and NC groups by measuring the cross-run consistency. As the community structure detected by cssNMF may vary from run to run due to different initializations, a solution with higher stability across runs is more likely to reflect the underlying community structure. In this sense, the cross-run stability could inform of the optimal value of k. Specifically, the community structure was detected for the AD and NC groups separately by using cssNMF under different values of k. The cross-run consistency was then measured by the cophenetic correlation coefficient, a commonly-used measure for determining the optimal number of components in NMF methods (Brunet et al., 2004). The cross-run consistency was computed with 20, 50 and 100 runs.

Reproducibility of the detected community structure

The split-half reproducibility was analyzed and compared between the two groups. The split-half reproducibility indicates whether the detected community structure is consistent across different subsets of participants. All the participants within each group were randomly divided into 2 halves and the community structure was derived for each half. The similarity between two community structures was measured by the cosine similarity. Before that, a graph matching procedure was performed to rearrange the order of the detected communities by using the Hungarian algorithm (Lovász and Plummer, 1986). The similarity was computed for each pair of matched communities and then averaged over all detected communities for each group. The split-half procedure was repeated 20 times for each group and the reported similarity was computed by averaging over all the repetitions.

Hierarchy of the detected communities

Then we investigated the differences between the AD and NC groups in terms of the hierarchy of their community structures. Specifically, for each group, we collected all the communities (i.e.,h_p) derived under different values of k and applied the agglomerative hierarchical clustering method (Hastie et al., 2009). The similarity between a pair of communities was measured by cosine similarity. A dendrogram depicting the hierarchical structure of these communities was derived as a result for each group.

Analysis of group-differences in network measures

Two types of network measures were compared between the AD and NC groups, which characterize the functional segregation and functional diversity of the overlapping community structure, respectively. For each measure, it was computed for each participant and compared between the two groups. Statistical significances of the differences in the mean values were tested by using the non-parametric permutation tests with 5000 permutations. For node-wise measures, correction for multiple comparisons was performed by constructing the null distribution using the maximum values among all the nodes for each permutation (Nichols and Holmes, 2002).

Functional segregation

In a modular network structure, functionally coherent nodes are clustered into a community, which may serve a specific purpose of the brain. In this study, two measures were used to characterize the functional segregation of the overlapping community structure derived by cssNMF, i.e., within-community connection strength and overall community strength. For each participant, the within-community connection strength was estimated by summing over the weights of connections within a community and then averaged over all the k communities:

$$\sum_{p=1}^{k} \|s_p^i h_p h_p^{\mathrm{T}}\|_1 \tag{2}$$

For each participant, the community strength was computed by summing the community strength (s_p^i) over all the k communities:

$$\sum_{p=1}^{k} s_p^i \tag{3}$$

A higher value of s_p^i indicates a more compact community, where the belonging connections are highly coherent.

Functional diversity

In an overlapping community structure, a node could participate in multiple communities serving diverse functions. To depict the node-wise functional diversity, we applied the Shannon's entropy measure (Shannon, 1948), as used in (Najafi et al., 2016). For a given participant i, the functional diversity of node j is calculated by

$$-\sum_{p=1}^{k} \mathrm{P}_{jp}^i \ln \mathrm{P}_{jp}^i \tag{4}$$

where $\mathrm{P}^i = \mathrm{H} * diag((s^i)^{\frac{1}{2}})$, and $s^i = (s_1^i, \ldots, s_k^i) \in \mathbb{R}^k$ contains the community strengths of participant i. Therefore, P_{jp}^i denotes the posterior probability of node j belonging to community p for participant i. The entropy measure achieves its maximum value when $\mathrm{P}_{jp} = \frac{1}{k}$ $(p = 1, \ldots, k)$.

Machine learning framework for AD detection

To further validate the differences in community structure between the AD and NC groups, we adopted a machine learning framework to classify AD patients and NCs. Specifically, we used the leave-one-out cross -validation (LOOCV) and the linear discriminant analysis (LDA) classifier. It means that in each fold one sample is used as the testing sample while all the rest samples are used as the training samples. The procedure is repeated until all samples have been chosen as the testing sample once and only once. Then classification accuracy is computed over all the testing samples. On the training set within each fold, we derived the community structure for the AD and NC group separately by using cssNMF, denoted by $H_{AD} \in \mathbb{R}^{n \times k}$ and $H_{NC} \in \mathbb{R}^{n \times k}$ respectively. Then we created a common template $H_c = (H_{AD}, H_{nc}) \in \mathbb{R}^{n \times 2k}$ and applied the template to all the participants in the training set with cssNMF to derive the community strengths, as well as to the participant in the testing set. The community strengths of each participant were used as features for classification. The accuracy, sensitivity and specificity were computed for the classification. Besides, permutation tests were conducted to evaluate the statistical significance of the derived accuracy against the chance level, where the features were randomly permuted before classification and the same procedure was

repeated 5000 times. A null distribution of the accuracies derived from the permutations was constructed and the p-value of the true accuracy was then determined by comparing to the $95th$ percentile of the null distribution.

Results

Parameter selection

Figs. 1A and **B** show the parameter selection results for the AD and NC groups, respectively. As can be seen, for both groups the cross-validation error stays relatively stable as β increases from 0 to 0.1, while it starts to increase quickly when β increases from 0.2 to 0.6. It indicates that the cssNMF method achieves an appropriate level of sparsity when $\beta = 0.1$. As β increases to larger than 0.6, the cross-validation error reaches a plateau, indicating a significant loss of generalizability due to the increased sparsity. In contrast, the selection of k is not straightforward from the result. When β changes from 0 to 0.4, the cross-validation error keeps dropping as k increases from 2 to 16, while when β is larger than 0.5, k seems to have little influence on the cross-validation error. Therefore, the sparsity level β was set to 0.1 for the both groups in the subsequent analyses.

Differences in terms of the number of communities

Fig. 2 shows the results of cross-run consistency for the AD and NC groups. Overall, the stability of the community structure achieves a high level of above 0.9 when $k > 2$ for both groups. For the AD group, the coefficient achieves the highest value when k is around 10. By contrast, the NC group attains the highest stability when k is around 14 and obtains another peak when k is around 6. In particular, the stability of the NC group is higher than that of the AD group at a finer scale of community structure where k is relatively large. For example, the cophenetic correlation coefficient values of AD are 0.9729, 0.9711, and 0.9748, and the values of the NC group are 0.9819, 0.9848, and 0.9856 with $k = 13$ when the number of runs are 20, 50, and 100, respectively. It indicates that the stability of the NC group is higher than that of the AD group at a finer scale of community structure where k is relatively large. Importantly, the trend of NC gradually rises as the k value increases, while AD tends to be stable when the k value is relatively small. This may indicate that the NC group tends to have a more modularized network structure than the AD group. Besides, the AD group reaches higher correlation levels with fewer communities from overall. For the AD group, the stability is not improved as the scale becomes finer, while the stability will gradually increase for the NC group. For the NC group, this trend indicates that there are still small structures in the large modules. Consequently, when the scale becomes delicate, the small structures are still stable and the value of the stability will increase. Compared with the AD group, the brain network of the NC group tends to be modular. This further supports our conclusion from another aspect.

Differences in terms of split-half reproducibility of community structure

The split-half reproducibility of the detected community structures for both groups is shown in **Fig. 3**. The reproducibility is averaged over all the 20 splits and the error bar denotes the standard deviation. On the whole, the reproducibility of the NC group is consistently higher than that of the AD group when k is larger than 6. A t-test revealed that the difference of split-half reproducibility between the two groups over all the values of k is significant ($p < 0.01$). The higher reproducibility of the NC group suggests that the

community structures are more stable and consistent across different cohorts of participants in the NC group than in the AD group.

Differences in terms of the hierarchy of the detected communities

To further explore where the differences between the two groups in the community structure lie, we analyzed the hierarchy of the communities detected over different values of k. Specifically, instead of choosing one community structure with a specific number of communities, we collected all the communities derived with k varying from 5 to 16 (i.e., 126 communities in total) and adopted agglomerative hierarchical clustering to reveal the hierarchical structure for each group. **Fig. 4A** displays the hierarchy of these communities for the AD and NC groups in the upper panel and lower panel respectively. The cut-off distance was set to 0.5 where 16 clusters of communities were identified for both groups. The clusters shown in **Fig. 4B** and **Fig. 4C** were derived by averaging over all communities within each cluster for the AD and NC groups respectively. Besides, in order to investigate which known resting-state networks were matched to the 16 clusters, we mapped these communities represented by membership matrices in **Fig. 4B** onto the human brain models for the two groups (the visual representation of all the communities identified is supplied in the supplementary material). And then we checked the distribution of these communities on the brain model to match the known resting-state network. Finally, we found these clusters roughly cover 11 common RSNs, including visual network (VN), orbitofrontal cortex (OFC), salience network (SN), DMN, execution control network (ECN), left/right frontoparietal networks (L/RFP), sensor-motor network (SEN), limbic system (LIM), ventral attention network (VAN) and basal ganglia (BG). The similarity between the two groups for each RSN computed by the cosine similarity was shown at the bottom. In particular, the SEN, frontoparietal (FP) and BG networks have significantly different hierarchies between the two groups than the other networks, as highlighted in **Figs. 4B** and **C**. Such differences in the community structures may indicate alterations of function in these areas.

We then depicted how the divergence between the AD and NC groups in the hierarchy structures happened for the FP, SEN and BG networks in **Fig. 5**. **Figs. 5A** and **B** show the communities related to FP and SEN networks for the AD and NC groups, respectively. For the AD group, C1-4 correspond to the clusters 8-11 in **Fig. 4**, which were detected and remained unchanged since $k = 15$, while for the NC group, C1-3 correspond to the clusters 8-10 in **Fig. 4**, which were detected and remained unchanged since $k = 14$. The main difference is that the parietal regions of the FP networks have much lower weights in the AD group than in the NC group, and were grouped into a separate community (C4) in the AD group. This may reflect alterations in the communication between the frontal and parietal regions in AD patients. **Figs. 5C** and **D** show the communities related to the BG network of the AD and NC groups, respectively. The BG network mainly covers the olfactory, putamen, pallidum and thalamus and caudate regions. For the AD group, the BG network was divided into 2 parts at $k = 12$ and further divided into 3 parts at $k = 16$, whereas for the NC group, the BG network was divided into smaller communities as a relatively smaller value of k and resulted in 4 parts at $k = 15$. This may indicate that the connections within the BG networks changes in the AD group, resulting in a less modular structure.

Differences in functional segregation

The functional segregation of the community structure is evaluated in terms of the within-community connection strength and community strength for both groups. The mean as well as the standard deviation

across all participants of the within-community connection strengths and the community strength are plotted in **Fig. 6A** and **Fig. 6B** respectively. Permutation tests reveal that the NC group has significantly and consistently stronger within-community connection strengths than the AD group under different values of k. Similarly, the community strength also achieves a significantly higher value in the NC group than in the AD group under different values of k. Such significantly reduced within-community strengths and community strengths of the AD group indicates that the AD patients may undergo an overall decline of the functionality of distinct communities, thus resulting in a loss of the functional separation of the brain network.

Differences in nodal functional diversity

Fig. 7 shows the results of nodal functional diversity of the AD and NC groups. **Fig. 7A** counts the number of nodes that show significantly larger functional diversity in the AD group (yellow) and in the NC group (blue) separately ($p < 0.05$, corrected) under each value of k. We observed that the NC group consistently had more nodes with larger functional diversity compared to the AD group under all values of k. **Fig. 7B** displays the nodes that are consistently (across at least 10 different values of k) reported to have higher functional diversity in the AD group (yellow, 9 nodes) and in the NC group (blue) separately. 29 nodes were found to have larger functional diversity in the NC group than in the AD group, covering the frontal, limbic, occipital, parietal, basal ganglia and temporal regions. This may suggest reduced functional diversity spanning all over the brain in the AD patients. By contrast, 9 nodes showed the opposite trend by having a higher functional diversity in the AD group. However, this may not suggest a true enhancement of the functional diversity of these nodes. As revealed by **Fig. 6**, the AD group showed overall reduced community strength. This may suggest that these regions have declined function, thus resulting in a blurred functional distinction.

Performance of community-structure-based classification

To further validate the differences in community structure between the AD and NC groups, we adopted a machine learning framework to use community structure-related features for AD detection. As described in the method section, the community strengths of each participant are used as features for classification. **Fig. 8** illustrates an example of the extracted features on the whole dataset with $k = 9$, where the similarity of the community structure between the two groups is 0.95 (**Fig. 8A**). Specifically, we derived the community structure for each group separately and combine the two community structures into a common template **Fig. 8B**. Then by using cssNMF with the common template, we derived the corresponding community strengths for each participant (**Fig. 8D**). We found that AD patients had larger weights for the communities in the AD part of the template, and vice versa for the NCs. The community strengths between the two groups showed a significant difference ($p < 0.05$, t-tests) for 15/18 communities, although most of the matched AD-NC community pairs had a relatively high similarity, as shown in **Fig. 8C**.

The LOOCV procedure was used when performing the classification. The advantage is that the testing participant was totally unseen when constructing the common template. **Figs. 9A**, **B** and **C** show the classification performance in terms of accuracy, sensitivity and specificity, respectively. We also tested the classification performance of the two networks that show substantial differences in the hierarchy of communities, i.e., the FP and BG networks. Overall, the accuracy was highest when jointly using the community strengths of the FP and BG networks (FP+BG), compared with using all communities or using FP or BG alone. Permutation tests showed that the classification accuracy when using the FP+BG feature

was significantly higher than chance level when $k > 6$ ($p < 0.05$), achieving above 60%. In the best case, the accuracy achieved 76.7% at $k = 15$. Similarly, the FP+BG feature also showed better performance in terms of sensitivity and specificity than using FP or BG feature alone. Besides, the BG network outperformed the FP network in sensitivity while vice versa for the specificity.

Discussion

In this work, we studied the overlapping community structure of AD patients. Our results showed that remarkable alterations occurred in the community structure of the brain functional networks of the AD patients, in terms of the optimal number, reproducibility and the hierarchy of the detected communities. Such alterations resulted in reduced brain functional segregation and integration in AD patients, which were measured by community strength and nodal functional diversity, respectively. Furthermore, using a LOOCV machine learning framework, we showed the potential for classifying AD patients and their healthy counterparts based on community structure-related features.

Our study focuses on the alterations in the overlapping community structure of functional brain network in AD patients, where the NASR and cssNMF algorithms were combined to detect the overlapping community structure. For both the NC and AD groups, we identified several well-recognized communities, such as DMN, visual, basal ganglia and frontal-parietal networks. These RSNs have been consistently reported by previous studies using different methods (Van den Heuvel and Pol, 2010; Yeo et al., 2014). However, the two groups exhibited different patterns in the relationship between the number of communities and the stability of the detected communities. Results showed that the NC group was more likely to achieve a stable community structure when the number of communities increased, indicated by the higher value of cross-run consistency **Fig. 2** and split-half reproducibility **Fig. 3**. It indicates that when more communities are identified, the assignment of the nodes is of less certainty in the AD patients, resulting in the decrease of the stableness. Namely, the brain functional network of the AD group is less organized than that of the NC group at a refined scale. This finding is in line with a previous MEG study, which has discovered a significant reduction in module count of the AD group in different frequency bands (de Haan et al., 2012). The decrease in the number of communities in the AD group may be due to the weakened functions of some brain areas, which makes the stability of the community on a finer scale decrease.

The hierarchy of the communities detected at different scales also showed the difference between the AD and NC groups, especially in the FP and BG networks **Fig. 4**. For the FP network, we found that the weights of regions in the frontal lobe were much higher in the AD patients than in the NCs. This is in line with the findings of several previous studies, which discovered increased connectivity in the frontal and prefrontal regions in AD patients (Wang et al., 2006; Supekar et al., 2008). These studies indicate that AD patients may depend on the increased connectivity weights in the frontal lobe to compensate for reduced temporal connectivity (Gould et al., 2006). For the BG network, we found that it was more modularized in the NC group than in the AD group. Abnormalities in regions related to the BG network have been reported by some previous studies. For example, structurally, MRI studies have found pathological changes in the thalamus, basal ganglia and caudate in patients with AD and MCI (de Jong et al., 2008; Ryan et al., 2013; Pini et al., 2016). Functionally, altered functional connectivity has been observed within the BG network (Binnewijzend et al., 2012) and for the thalamus (Li et al., 2015). The difference may be caused by the atrophy of the accumbens and thalamus in the BG network in AD patients. Taken together, the abnormalities

in FP and BG networks may be important biomarkers for the detection of AD patients. These findings may clarify that the combination of the cssNMF and agglomerative hierarchical clustering is a promising method to study the pathological changes in the overlapping and hierarchical community structures in AD patients.

In terms of functional segregation and diversity, on the one hand, the AD group shows significantly lower within-community connection strength and community strength under different values of k than the NC group **Fig. 6**, implying reduced functional segregation of the brain functional network of the AD patients. Several previous studies have also reported declined functional segregation by using different measures, such as intra-modular connection loss (de Haan et al., 2012) and lower clustering coefficient (Supekar et al., 2008; Brier et al., 2014). On the other hand, we found that the functional diversity remarkably reduces in nodes spreading over the frontal, parietal, occipital, temporal, basal ganglia and limbic regions of the AD group, as shown in **Fig. 7**. Similar abnormality has also been observed in non-overlapping community structures, indicated by reduced functional integration (Liu et al., 2013; Dai and He, 2014). Clinically, the most obvious features of AD patients are the decline in memory and execution. Among them, memory depends on the information flow within certain specific brain regions. Namely, it is related to the functional segregation ability. The execution ability depends on the information integration among all brain regions, which is associated with the function integration ability of the entire brain. This is in line with our finding that the functional segregation and integration are reduced in the AD group, which indicates that our approaches are effective for measuring the difference between the NC group and the AD group.

Discovering group differences between AD patients and NCs deepens our understanding of AD. Furthermore, a more practical and urgent task may be to find stable biomarkers to aid in the diagnosis on an individual basis. In this study, the community structure-based at the individual level was used for AD classification. It can obtain more than 60% classification accuracy rates with the statistically significant when community strengths are used as features. Notaly, the best accuracy can achieve 76.7% at $k = 15$ when using the FP+BG feature. Many studies have implemented the AD classification using neuroimaging data of different modalities such as MRI or fMRI (Rathore et al., 2017). In particular, functional connection values and graph theory metrics are the most commonly used features in AD classification based on fMRI data. An fMRI study found that compared to graph metrics, function connection values have more recognition ability for AD patients. However, it is usually necessary to reduce the feature dimension by using supervised or unsupervised methods before classification because the functional connection has high dimensionality. Supervised methods often need to be combined with cross-validation to reduce feature dimensionality, leading to retaining different features in different cross-validation folds. While the features extracted by commonly used unsupervised methods such as principal component analysis (PCA) often lack intuitive neurophysiological meaning. In this study, the cssNMF algorithm is used as both an unsupervised dimensionality reduction method and a feature extraction method. In addition, the community strength extracted by the cssNMF method as the AD classification feature has clear physical and neurophysiological significance, which makes the classification results easier to interpret.

The main limitation of this work is that the sample size of both the AD group and the NC group is relatively small. This may cause a lack of generalizability of the findings of this work. To further validate the differences of community structure identified in this work, we performed a machine learning framework with LOOCV to adopt the community structure derived features for AD detection. The results showed that these features could achieve an accuracy of 76.7% in the best case. In particular, using the features related

to the FP and BG networks achieved the best overall accuracy, which further supported our finding. These results demonstrated the potentials for using community structure-related features for the detection of AD. Many efforts have been made to design machine learning frameworks for AD or MCI detection, by using various features extracted from structural and functional brain images (Rathore et al., 2017). Future work could incorporate different types of features extracted from multi-modal imaging data to further improve the classification accuracy. Besides, the head motion has a significant effect on measures of functional connectivity and community identification. Therefore, it is necessary to consider the head motion correction models to reduce motion artifact in data preprocessing. For example, confound regression strategies may be adopted to mitigate the impact of head motion on functional connectivity and community identification to improve our research in the future work (Ciric et al., 2017). Furthermore, a more refined classification of the AD group is a problem worth exploring in the follow-up work. Lastly, we used one preprocessing pipeline to implement the data pre-processing and one anatomical atlas to define the ROIs in this work. Different pre-processing steps, such as whether to perform global signal regression or scrubbing, may affect the consistency of the value. In addition, it showed that using different brain parcellations could significantly change the findings. Therefore, the reliability and reproducibility of the findings in this work need to be further validated by using more than one preprocessing pipeline and other brain parcellations.

In this study, we investigated the overlapping community structure of AD patients. An approach using NASR with cssNMF was used to detect the overlapping community structure and preserve the individual differences in community strength. We found that the AD patients and the NCs showed remarkable differences in many aspects of the overlapping community structure, including the optimal number of communities, reproducibility, hierarchy of communities detected at different scales, network functional segregation and nodal functional diversity. Furthermore, a machine learning framework with LOOCV was deployed for AD detection based on the detected community strength, which achieved classification accuracy of 76.7% in the best case where the features related to BG and FP networks were used. We believe that this study provides novel insights into the brain functional network organization in AD and shows the potential of the community structure-related features to serve as biomarkers for AD diagnosis.

Acknowledgments

This work was supported by the National Natural Science Foundation of China under Grants 62176054 and 61773114, and the University Synergy Innovation Program of Anhui Province under Grant GXXT-2020-015.

Data collection and sharing for this project was funded by the Alzheimer's Disease Neuroimaging Initiative (ADNI) (National Institutes of Health Grant U01 AG024904) and DOD ADNI (Department of Defense award number W81XWH-12-2-0012). ADNI is funded by the National Institute on Aging, the National Institute of Biomedical Imaging and Bioengineering, and through generous contributions from the following: AbbVie, Alzheimer's Association; Alzheimer's Drug Discovery Foundation; Araclon Biotech; BioClinica, Inc.; Biogen; Bristol-Myers Squibb Company; CereSpir, Inc.; Cogstate; Eisai Inc.; Elan Pharmaceuticals, Inc.; Eli Lilly and Company; EuroImmun; F. Hoffmann-La Roche Ltd and its affiliated company Genentech, Inc.; Fujirebio; GE Healthcare; IXICO Ltd.; Janssen Alzheimer Immunotherapy Research & Development, LLC.; Johnson & Johnson Pharmaceutical Research & Development LLC.; Lumosity; Lundbeck; Merck & Co., Inc.; Meso Scale Diagnostics, LLC.; NeuroRx Research; Neurotrack Technologies; Novartis Pharmaceuticals Corporation; Pfizer Inc.; Piramal Imaging; Servier; Takeda Pharmaceutical Company; and Transition Therapeutics. The

Canadian Institutes of Health Research is providing funds to support ADNI clinical sites in Canada. Private sector contributions are facilitated by the Foundation for the National Institutes of Health (www.fnih.org). The grantee organization is the Northern California Institute for Research and Education, and the study is coordinated by the Alzheimer's Therapeutic Research Institute at the University of Southern California. ADNI data are disseminated by the Laboratory for Neuro Imaging at the University of Southern California.

Declaration of interest

We wish to confirm that there are no known conflicts of interest associated with this manuscript and there has been no significant financial support for this work that could have influenced its outcome.

Role of the funding source

The research was conducted in the absence of any commercial or financial relationships that could be construed as a potential conflict of interest.

References

Binnewijzend, M.A., Schoonheim, M.M., Sanz-Arigita, E., Wink, A.M., Van der Flier, W.M., Tolboom, N., Adriaanse, S.M., Damoiseaux, J.S., et al, 2012. Resting-state fMRI changes in Alzheimer's disease and mild cognitive impairment. Neurobiol. Aging 33, 2018–2028.

Biswal, B., Zerrin Yetkin, F., Haughton, V.M., Hyde, J.S., 1995. Functional connectivity in the motor cortex of resting human brain using echo-planar MRI. Magn. Reson. Med. 34, 537–541.

Brier, M.R., Thomas, J.B., Fagan, A.M., Hassenstab, J., Holtzman, D.M., Benzinger, T.L., Morris, J.C., Ances, B.M., 2014. Functional connectivity and graph theory in preclinical Alzheimer's disease. Neurobiol. Aging 35, 757–768.

Brunet, J.P., Tamayo, P., Golub, T.R., Mesirov, J.P., 2004. Metagenes and molecular pattern discovery using matrix factorization. Proc. Natl. Acad. Sci. 101, 4164–4169.

Ciric, R., Wolf, D.H., Power, J.D., Roalf, D.R., Baum, G.L., Ruparel, K., Shinohara, R.T., Elliott, M.A., et al, 2017. Benchmarking of participant-level confound regression strategies for the control of motion artifact in studies of functional connectivity. Neuroimage 154, 174–187.

Cole, M.W., Reynolds, J.R., Power, J.D., Power, J.D., Repovs, G., Braver, T.S., 2013. Multi-task connectivity reveals flexible hubs for adaptive task control. Nat. Neurosci. 16, 1348–U247.

Contreras, J.A., Avena-Koenigsberger, A., Risacher, S.L., West, J.D., Tallman, E., McDonald, B.C., Farlow, M.R., Apostolova, L.G., et al, 2019. Resting state network modularity along the prodromal late onset alzheimer's disease continuum. NeuroImage-Clin. 22, 101687.

Crossley, N.A., Mechelli, A., Vértes, P.E., Winton-Brown, T.T., Patel, A.X., Ginestet, C.E., McGuire, P., Bullmore, E.T., 2013. Cognitive relevance of the community structure of the human brain functional coactivation network. Proc. Natl. Acad. Sci. 110, 11583–11588.

Dai, Z., He, Y., 2014. Disrupted structural and functional brain connectomes in mild cognitive impairment and Alzheimer's disease. Neurosci. Bull. 30, 217–232.

Dennis, E.L., Thompson, P.M., 2014. Functional brain connectivity using fMRI in aging and Alzheimer's disease. Neuropsychol. Rev. 24, 49–62.

Fornito, A., Zalesky, A., Michael, B., 2015. The connectomics of brain disorders. Nat. Rev. Neurosci. 16, 159–172.

Gould, R.L., Arroyo, B., Brown, R.G., Owen, A.M., Bullmore, E.T., Howard, R.J., 2006. Brain mechanisms of successful compensation during learning in alzheimer disease. Neurology 67, 1011–1017.

de Haan, W., Van der Flier, W.M., Koene, T., Smits, L.L., Scheltens, P., Stam, C.J., 2012. Disrupted modular brain dynamics reflect cognitive dysfunction in Alzheimer's disease. Neuroimage 59, 3085–3093.

Hastie, T., Tibshirani, R., Friedman, J., 2009. Unsupervised learning, in: The elements of statistical learning. Springer, pp. 485–585.

Van den Heuvel, M.P., Pol, H.E.H., 2010. Exploring the brain network: a review on resting-state fMRI functional connectivity. Eur. Neuropsychopharmacol. 20, 519–534.

Hojjati, S.H., Ebrahimzadeh, A., Babajani-Feremi, A., 2019. Identification of the early stage of alzheimer's disease using structural mri and resting-state fMRI. Front. Neurol. 10, 904.

Jack, C.R., Bernstein, M.A., Fox, N.C., Thompson, P., Alexander, G., Harvey, D., Borowski, B., Britson, P.J., et al, 2008. The Alzheimer's disease neuroimaging initiative (ADNI): MRI methods. J. Magn. Reson. Imaging 27, 685–691.

John, M., Ikuta, T., Ferbinteanu, J., 2017. Graph analysis of structural brain networks in Alzheimer's disease: beyond small world properties. Brain Struct. Funct. 222, 923–942.

de Jong, L.W., Van der Hiele, K., Veer, I.M., Houwing, J.J., Westendorp, R.G.J., Bollen, E.L.E.M., de Bruin, P.W., Middelkoop, H.A.M., et al, 2008. Strongly reduced volumes of putamen and thalamus in Alzheimer's disease: an MRI study. Brain 131, 3277–3285.

Li, H.J., Hou, X.H., Liu, H.H., Yue, C.L., He, Y., Zuo, X., 2015. Toward systems neuroscience in mild cognitive impairment and Alzheimer's disease: a meta-analysis of 75 fMRI studies. Hum. Brain Mapp. 36, 1217–1232.

Li, X., Gan, J.Q., Wang, H., 2018. Collective sparse symmetric non-negative matrix factorization for identifying overlapping communities in resting-state brain functional networks. Neuroimage 166, 259–275.

Li, X., Wang, H., 2015. Identification of functional networks in resting state fMRI data using adaptive sparse representation and affinity propagation clustering. Front. Neurosci. 9.

Li, Y., Liu, J., Gao, X., Jie, B., Minjeong, K., Pew-Thian, Y., Chong-Yaw, W., Shen, D., 2019. Multimodal hyper-connectivity of functional networks using functionally-weighted LASSO for MCI classification. Med. Image Anal. 52, 80–96.

Lin, Y., Ma, J., Gu, Y., Yang, S., Li, L.M.W., Dai, Z., 2018. Intrinsic overlapping modular organization of human brain functional networks revealed by a multiobjective evolutionary algorithm. Neuroimage 181, 430–445.

Liu, Y., Yu, C., Zhang, X., Liu, J., Duan, Y., Alexander-Bloch, A.F., Liu, B., Jiang, T., et al, 2013. Impaired long distance functional connectivity and weighted network architecture in Alzheimer's disease. Cereb. Cortex 24, 1422–1435.

Lovász, L., Plummer, M.D., 1986. Matching theory. Ann. Discret. Math 29.

Mirzaei, S., Soltanian-Zadeh, H., 2019. Overlapping brain community detection using bayesian tensor decomposition. J. Neurosci. Meth. 318, 47–55.

Najafi, M., McMenamin, B.W., Simon, J.Z., Pessoa, L., 2016. Overlapping communities reveal rich structure in large-scale brain networks during rest and task conditions. Neuroimage 135, 92–106.

Nichols, T.E., Holmes, A.P., 2002. Nonparametric permutation tests for functional neuroimaging: a primer with examples. Hum. Brain Mapp. 15, 1–25.

Noroozi, A., Rezghi, M., 2020. A tensor-based framework for rs-fMRI classification and functional connectivity construction. Front. Neuroinform. 14, 46.

O'Reilly, J.X., Beckmann, C.F., Tomassini, V., Ramnani, N., Johansen-Berg, H., 2010. Distinct and overlapping functional zones in the cerebellum defined by resting state functional connectivity. Cereb. Cortex 20, 953–965.

Palla, G., Derényi, I., Farkas, I., Vicsek, T., 2005. Uncovering the overlapping community structure of complex networks in nature and society. Nature 435, 814.

Pievani, M., de Haan, W., Wu, T., Seeley, W.W., Frisoni, G.B., 2011. Functional network disruption in the degenerative dementias. Lancet Neurol. 10, 829–843.

Pini, L., Pievani, M., Bocchetta, M., Altomare, D., Bosco, P., Cavedo, E., Galluzzi, S., Marizzoni, M., et al, 2016. Brain atrophy in Alzheimer's disease and aging. Ageing Res. Rev. 30, 25–48.

Power, J.D., Cohen, A.L., Nelson, S.M., Wig, G.S., Barnes, K.A., Church, J.A., Vogel, A.C., Laumann, T.O., et al, 2011. Functional network organization of the human brain. Neuron 72, 665–678.

Prasad, G., Joshi, S.H., Nir, T.M., Toga, A.W., Thompson, P.M., (ADNI), A.D.N.I., 2015. Brain connectivity and novel network measures for Alzheimer's disease classification. Neurobiol. Aging 36, S121–S131.

Rathore, S., Habes, M., Iftikhar, M.A., Shacklett, A., Davatzikos, C., 2017. A review on neuroimaging-based classification studies and associated feature extraction methods for Alzheimer's disease and its prodromal stages. Neuroimage 155, 530–548.

Ryan, N.S., Keihaninejad, S., Shakespeare, T.J., Lehmann, M., Crutch, S.J., Malone, I.B., Thornton, J.S., Mancini, L., et al, 2013. Magnetic resonance imaging evidence for presymptomatic change in thalamus and caudate in familial Alzheimer's disease. Brain 136, 1399–1414.

Shannon, C.E., 1948. A mathematical theory of communication. Bell Syst. Tech. J. 27, 623–656.

Sporns, O., 2013. Network attributes for segregation and integration in the human brain. Curr. Opin. Neurobiol. 23, 162–171.

Sun, L., Xue, Y., Zhang, Y., Zhang, L., Liu, M., 2021. Estimating sparse functional connectivity networks via hyperparameter-free learning model. Artif. Intell. Med. 111, 102004.

Supekar, K., Menon, V., Rubin, D., Musen, M., Greicius, M.D., 2008. Network analysis of intrinsic functional brain connectivity in Alzheimer's disease. PLoS Comput. Biol. 4, e1000100.

Teipel, S., Drzezga, A., Grothe, M.J., Barthel, H., Chetelat, G., Chuff, N., Skudlarski, P., Cavedo, E., et al, 2015. Multimodal imaging in alzheimer's disease: validity and usefulness for early detection. Lancet Neurol. 14, 1037–1053.

Tzourio-Mazoyer, N., Landeau, B., Papathanassiou, D., Crivello, F., Etard, O., Delcroix, N., Mazoyer, B., Joliot, M., 2002. Automated anatomical labeling of activations in SPM using a macroscopic anatomical parcellation of the MNI MRI single-subject brain. Neuroimage 15, 273–289.

de Vos, F., Koini, M., Schouten, T.M., Seiler, S., Van der Grond, J., Lechner, A., Schmidt, R., de Rooij, M., et al, 2018. A comprehensive analysis of resting state fMRI measures to classify individual patients with Alzheimer's disease. Neuroimage 167, 62–72.

Wang, L., Zang, Y., He, Y., Liang, M., Zhang, X., Tian, L., Wu, T., Jiang, T., et al, 2006. Changes in hippocampal connectivity in the early stages of Alzheimer's disease: evidence from resting state fMRI. Neuroimage 31, 496–504.

Wen, X., Zhang, H., Li, G., Liu, M., Yin, W., Lin, W., Zhang, J., Shen, D., 2018. First-year development of modules and hubs in infant brain functional networks. Neuroimage 185, 222–235.

Wu, K., Taki, Y., Sato, K., Sassa, Y., Inoue, K., Goto, R., Okada, K., Kawashima, R., et al, 2011. The overlapping community structure of structural brain network in young healthy individuals. PLoS ONE 6, e19608.

Xue, C., Sun, H., Hu, G., Qi, W., Yue, Y., Rao, J., Yang, W., Xiao, C., et al, 2020. Disrupted patterns of rich-club and diverse-club organizations in subjective cognitive decline and amnestic mild cognitive impairment. Front. Neurosci. 14, 984.

Yan, C., Zang, Y., 2010. DPARSF: a MATLAB toolbox for "pipeline" data analysis of resting-state fMRI. Front. Syst. Neurosci. 4.

Yeo, B.T., Krienen, F.M., Chee, M.W., Buckner, R.L., 2014. Estimates of segregation and overlap of functional connectivity networks in the human cerebral cortex. Neuroimage 88, 212–227.

Yeo, B.T.T., Krienen, F.M., Sepulcre, J., Sabuncu, M.R., Lashkari, D., Hollinshead, M., Roffman, J.L., Smoller, J.W., et al, 2011. The organization of the human cerebral cortex estimated by intrinsic functional connectivity. J. Neurophysiol. 106, 1125–1165.

The figure captions

Figure 1: Parameter selection for cssNMF by grid search using cross-validation. (A) and (B) are the test error results derived for the AD group and the NC group respectively.

Figure 2: Cross-run consistency (cophenetic correlation coefficient) of the detected community structure under different values of k. (A) and (B) are the results derived for the AD group and the NC group respectively. The cross-run consistency is measured by the cophenetic correlation coefficient with the number of runs of 20, 50 and 100 separately.

Figure 3: Split-half reproducibility of detected community structures under different values of k for the AD and NC groups. The similarity of community structures is calculated by using the cosine similarity. The reproducibility is averaged over all the 20 repetitions within each group for each value of k, where the error bar indicates the standard deviation.

Figure 4: Hierarchy structure of the communities detected over different values of k. (A) displays the dendrogram of the hierarchical structure of the communities derived with k varying from 5 to 16 for AD and NC in the upper panel and lower panel respectively. The X axis represents the different clusters, and Y axis represents the distance between the clusters. The cut-off distance is set to 0.5, where all communities are merged into 16 clusters for each group. These clusters cover 11 common RSNs, including visual network (VN), orbitofrontal cortex (OFC), salience network (SN), DMN, execution control network (ECN), left/right frontoparietal network (L/RFP), sensor-motor network (SEN), limbic system (LIM), ventral attention network (VAN) and basal ganglia (BG). The similarity for each RSN between the two groups is shown at the bottom and each RSN is marked by one color. (B) and (C) show the resultant clusters by averaging the communities within each cluster for the AD and NC groups, respectively. The column represents the community index and the row represents the node index in the matrix represention. The red boxes highlight the differences between the two groups in terms of within-cluster hierarchical structure.

Figure 5: The visualization of differences in the FP and BG networks between the AD and NC groups via the BrainNet Viewer toolbox. (A) shows the communities related to FP and SEN networks identified at $k = 15$ for the AD group, where C1-4 correspond to the clusters 8-11 in Fig. 4, respectively. (B) shows the communities related to FP and SEN networks identified at $k = 14$ for the NC group, where C1-3 correspond to the clusters 8-10 in Fig. 4, respectively. (C) shows the communities related to BG networks identified at $k = 12, 16$ for the AD group, where C1-3 correspond to the clusters 14-16 in Fig. 4, respectively. (D) shows the communities related to BG networks identified at $k = 11, 13, 15$ for the NC group, where C1-4 correspond to the clusters 13-16 in Fig. 4, respectively.

Figure 6: Comparison between the AD and NC groups in within-community connection strengths and community strength under different values of k. (A) and (B) display the results of the within-community connections strengths and community strength, respectively. The mean value across all participants as well

as the standard deviation is plotted for each value of k. The star at the bottom indicates that there is a significant difference between the two groups with $p < 0.05$ (AD>NC marked in blue and NC>AD marked in red).

Figure 7: Comparison between the AD and NC groups in node functional diversity. (A) displays the number of nodes that show significantly different functional diversity between the two groups ($p < 0.05$, corrected), under different values of k. (B) plots the nodes that have consistently larger functional diversity in the AD group (yellow) and in the NC group (blue) across at least 10 different values of k, this representation is obtained by the BrainNet Viewer toolbox.

Figure 8: An example of extracting community strengths as features on the whole dataset. (A) displays the similarity between the community structure derived on the AD and NC groups under different values of k. $k = 9$ is selected as an example for illustrating the extracted features. (B) shows the community structure derived for the AD and NC groups in the left and right panel, respectively. The rows and columns in the matrix represention indicate the node index and the community index, respectively. (C) shows the similarity between each AD-NC community pairs (matched). (D) shows the extracted features, i.e., the strengths corresponding to the communities in (B) for each participant. The rows and columns in the matrix represention indicate the participant index and the community index, respectively. The red star under each community indicate that the difference in community strength between the two groups is significant ($p < 0.05$, t-tests) for that community.

Figure 9: Performance of the community structure-based classification framework under different values of k. (A) shows the classification accuracy under different values of k. "All" means the community strengths of all communities are used as features. "FP" and "BG" denote the only community strength of the FP network or the BG network is used, respectively. "FP+BG" means the community strengths of both the FP and BG networks are used as features. The red star on top of each condition indicates that the true accuracy is significantly larger than the chance level, revealed by a permutation test ($p < 0.05$). (B) and (C) show the corresponding sensitivity and specificity respectively.